

Molecular Quantum Transformer

Yuichi Kamata,^{*} Quoc Hoan Tran,[†] Yasuhiro Endo, and Hirotaka Oshima

Quantum Laboratory, Fujitsu Research, Fujitsu Limited, Kawasaki, Kanagawa 211-8588, Japan

The Transformer model, renowned for its powerful attention mechanism, has achieved state-of-the-art performance in various artificial intelligence tasks but faces challenges such as high computational cost and memory usage. Researchers are exploring quantum computing to enhance the Transformer’s design, though it still shows limited success with classical data. With a growing focus on leveraging quantum machine learning for quantum data, particularly in quantum chemistry, we propose the Molecular Quantum Transformer (MQT) for modeling interactions in molecular quantum systems. By utilizing quantum circuits to implement the attention mechanism on the molecular configurations, MQT can efficiently calculate ground-state energies for all configurations. Numerical demonstrations show that in calculating ground-state energies for H_2 , LiH , BeH_2 , and H_4 , MQT outperforms the classical Transformer, highlighting the promise of quantum effects in Transformer structures. Furthermore, its pretraining capability on diverse molecular data facilitates the efficient learning of new molecules, extending its applicability to complex molecular systems with minimal additional effort. Our method offers an alternative to existing quantum algorithms for estimating ground-state energies, opening new avenues in quantum chemistry and materials science.

I. INTRODUCTION

The Transformer model [1] has been recognized as a remarkable advancement in artificial intelligence. Its key power lies in its “attention mechanism”, which discerns the relative importance of different parts of its input and the connection strengths between them. This mechanism has been successfully applied to both natural language processing and visual object recognition tasks, delivering state-of-the-art performance across a variety of datasets. Despite these successes, the current implementation of the Transformer faces several challenges, including high computational costs, substantial memory requirements, the necessity for large datasets, and a vast number of training parameters. These limitations have prompted researchers to explore improved Transformer designs.

The marriage of quantum computing and machine learning has given rise to the field of quantum machine learning (QML) [2–5], which aims to leverage quantum computers to tackle problems that are infeasible for classical computers. In this context, efforts have been made to develop quantum versions of the Transformer model. A significant advancement in quantum neural networks (QNNs) involves integrating the self-attention mechanism by encoding query and key vectors as quantum states using parametric quantum circuits (PQCs). This adaptation enables quantum analogs of the classical self-attention framework, though various approaches differ in their implementation. One straightforward extension replaces the classical inner-product self-attention with the overlap of quantum states [6], but this method struggles to scale effectively for capturing correlations in large datasets due to its computational complexity. To address this limitation, an alternative employs classical Gaussian

projections of query and key quantum states, enhancing scalability while retaining essential features [7]. Other quantum self-attention variants include quantum vision Transformers [8] as an end-to-end approach that leverages analog encoding with quantum random access memory (qRAM) [9], and hybrid classical-quantum methods [10, 11] to reduce the time complexity of computing query-key dot products. Additionally, some proposals diverge from inner-product-based attention entirely, opting instead to mix tokens directly in Hilbert space to model correlations without explicitly calculating query-key dot products [12, 13]. Despite these innovative adaptations, these quantum self-attention implementations have demonstrated limited performance on tasks involving classical data, such as text and image classification, highlighting challenges in translating the advantages of quantum Transformer to practical applications.

In recent years, there has been a growing recognition within the research community that classical data, such as text and images, do not inherently require quantum effects for processing. Consequently, there is a shift towards employing QML methods that exploit quantum effects on data originating from quantum systems [14]. One promising yet underexplored area is the application of QML methods in quantum chemistry, where QML holds the potential to determine molecular and material properties more efficiently than traditional quantum computational chemistry algorithms.

A central focus in quantum computational chemistry is the electronic structure problem, which involves calculating the electronic Hamiltonian’s ground-state energy while assuming the molecule’s nuclei remain fixed. Among the most studied algorithms for this problem are the Variational Quantum Eigensolver (VQE) [15, 16] for Noisy Intermediate-Scale Quantum (NISQ) devices and Quantum Phase Estimation (QPE) [17, 18] for fault-tolerant quantum computers. While these approaches show promise, they face practical limitations. For instance, estimating the ground-state energy of $FeMoCo$, a

^{*} kamata.yuichi@fujitsu.com

[†] tran.quochoan@fujitsu.com

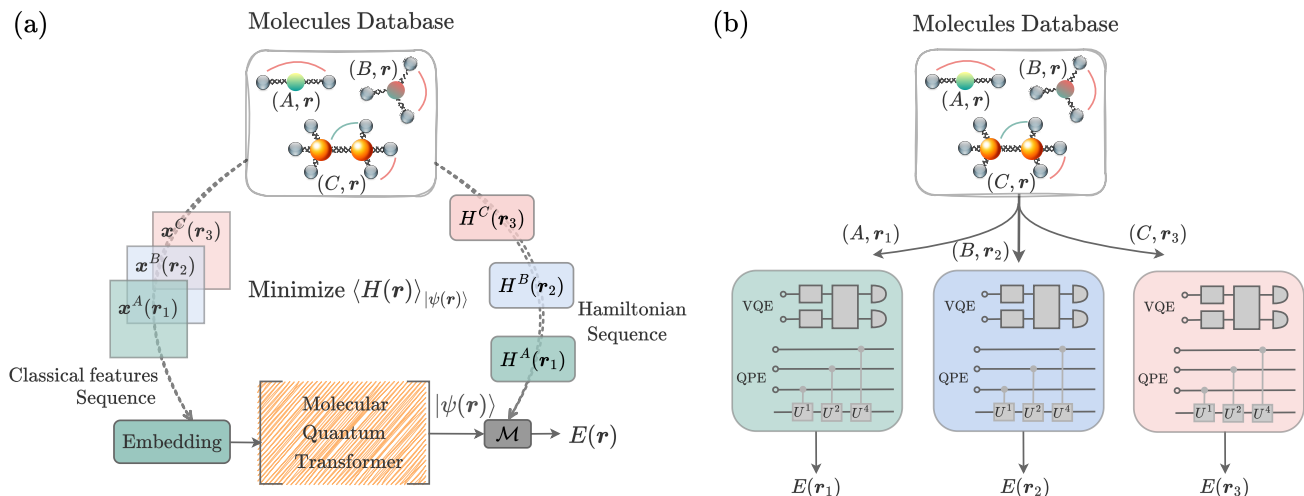


FIG. 1. Overview of the Molecular Quantum Transformer (MQT) model for the ground-state energy calculation across various molecules and their configurations, and the comparison with traditional methods. (a) For each molecule A, B, C, \dots and its associated configuration $\mathbf{r}_1, \mathbf{r}_2, \mathbf{r}_3, \dots$, the MQT receives a corresponding classical features sequence $\mathbf{x}^A(\mathbf{r}_1), \mathbf{x}^B(\mathbf{r}_2), \mathbf{x}^C(\mathbf{r}_3), \dots$ through an embedding process. Leveraging a quantum attention mechanism, the MQT models the complex interactions and correlations within the molecular system. The output of the MQT is a sequence of quantum states $|\psi^A(\mathbf{r}_1)\rangle, |\psi^B(\mathbf{r}_2)\rangle, |\psi^C(\mathbf{r}_3)\rangle, \dots$, which reflects these correlations in a variational representation of the estimated ground states for $(A, \mathbf{r}_1), (B, \mathbf{r}_2), (C, \mathbf{r}_3), \dots$, respectively. The corresponding Hamiltonian $H^A(\mathbf{r}_1), H^B(\mathbf{r}_2), H^C(\mathbf{r}_3), \dots$, derived from quantum mechanics are transformed into measurable operators to be measured on $|\psi^A(\mathbf{r}_1)\rangle, |\psi^B(\mathbf{r}_2)\rangle, |\psi^C(\mathbf{r}_3)\rangle, \dots$. During training, the optimization process adjusts the variational parameters in both the MQT and the embedding process to minimize the expectation value $\langle H(\mathbf{r}) \rangle_{|\psi(\mathbf{r})\rangle}$ across various molecules and a range of \mathbf{r} values. In the evaluation phase, given a molecule, the MQT can provide an estimator of ground-state energy $E(\mathbf{r})$ for any configuration \mathbf{r} . (b) In contrast, traditional methods such as VQE or QPE require an independent and computationally expensive solver for each molecule and configuration \mathbf{r} .

well-known and practical benchmark in quantum chemistry, would require a fault-tolerant quantum computer with millions of physical qubits operating for nearly four days using QPE [19]. In contrast, VQE can utilize fewer, noisier qubits, but its scalability is hindered by the extensive measurement demands during optimization, particularly for large-scale molecular systems [20, 21].

In practical quantum chemistry, estimating the ground-state energy for a single molecular configuration is often insufficient. Determining dynamic and structural properties, such as reaction barriers and optimal geometries, necessitates exploring multiple configurations. This requires knowledge of a family of ground states for a series of Hamiltonians parameterized by variables like nuclear coordinates and electron-nucleus distances. Consequently, one must compute numerous ground states with corresponding energies over a potential energy surface. However, a straightforward approach, such as independently running QPE or VQE for each configuration, incurs prohibitive computational costs. To address this, meta-based approaches leverage classical ML to optimize circuit parameters across multiple configurations simultaneously, as seen in Meta-VQE [22]. Another intriguing approach is the use of generative QML to produce ground states with PQCs learning from quantum data [23]. Nevertheless, these methods lack adaptability to varying molecule types and Hamiltonian forms and

fail to capture correlations as effectively as Transformer-based models.

In this paper, we introduce the Molecular Quantum Transformer (MQT), a Quantum Transformer model designed to calculate molecular ground-state energies [Fig. 1(a)]. The MQT leverages attention mechanisms implemented through quantum circuits, enabling efficient modeling of complex interactions and correlations within molecular quantum systems. By training on random molecular configurations at each iteration, the MQT captures these interactions, allowing it to generalize and obtain ground-state energies across diverse configurations. The MQT enables the simultaneous learning of ground-state energies for molecules across a range of bond lengths within a single model, providing greater resource efficiency compared to independently executing QPE or VQE for each molecular configuration [Fig. 1(b)]. We also compare MQT to a classical Transformer model under identical conditions of model dimensionality, demonstrating the superior performance of MQT over its classical counterpart. Furthermore, the MQT can be utilized to learn new molecules efficiently through pretraining with diverse molecular data. This capability is particularly significant, as it allows for the applications of MQT in complex molecules with minimal effort, leveraging well-known molecular data.

II. MODEL

A. The electronic structure problem

We consider a complex quantum many-body system in which multiple electrons and nuclei interact with each other through Coulomb interactions. Since the nuclei are thousands of times heavier than the electrons, they hardly move under the attraction from the electrons and can be regarded as fixed at coordinates \mathbf{R}_m (Born-Oppenheimer approximation). The wave function where N electrons move around M (fixed) nuclei can be written as $\psi(\mathbf{r}_1, \mathbf{r}_2, \dots, \mathbf{r}_N)$, and the Hamiltonian H for the electrons can be expressed in Hartree atomic units as follows in the following simplified form (first quantization):

$$H(\mathbf{R}) = -\sum_{i=1}^N \frac{1}{2} \nabla_i^2 + \sum_{i<j}^N \frac{1}{|\mathbf{r}_i - \mathbf{r}_j|} - \sum_{i=1}^N \sum_{m=1}^M \frac{Z_m}{|\mathbf{r}_i - \mathbf{R}_m|}. \quad (1)$$

Solving the Schrödinger equation $H\psi = E\psi$ with the energy eigenvalue E of H to determine the electronic state of a quantum many-body system is known as the molecular electronic problem. This problem is crucial for materials design and drug discovery but remains a central challenge in quantum chemistry due to the exponential complexity of quantum many-body systems.

Advanced methods in classical computation have advanced our ability to approximate solutions to the molecular electronic problem. These include the configuration interaction (CI) method, which constructs wavefunctions as linear combinations of Slater determinants to capture electron correlation [24]; the coupled cluster (CC) expansion [25], which employs an exponential ansatz to account for electron correlation more efficiently than CI; and Møller-Plesset perturbation theory (MP) [26], which treats electron correlation as a perturbative correction to the Hartree-Fock solution. Density functional theory (DFT) [27], another cornerstone method, focuses on electron density rather than the wave function, offering a balance between accuracy and computational cost. The quantum Monte Carlo (QMC) [28] method provides a stochastic approach to sampling the wavefunction, achieving high accuracy for small systems despite its computational intensity. The density matrix renormalization group (DMRG) method [29], originally developed for condensed matter physics, has been adapted to quantum chemistry and is particularly effective for systems with strong electron correlation [30].

In parallel, quantum computers have emerged as a promising alternative platform for addressing the molecular electronic problem, leveraging their ability to naturally represent and manipulate quantum states. Quantum computers offer the potential to overcome the limitations of classical algorithms, particularly for preparing ground states of quantum many-body systems that are intractable with traditional methods. Significant efforts have focused on developing quantum algorithms tailored

to this task. Quantum Phase Estimation (QPE) [17, 18] extracts eigenvalues of a Hamiltonian with exponential precision, provided a good initial state is available. Variational Quantum Eigensolver (VQE) [15, 16] adopts a hybrid quantum-classical approach to variationally minimize the energy expectation value. Other approaches include adiabatic quantum computing, which evolves a system from a simple initial Hamiltonian to the target Hamiltonian [31]; imaginary-time evolution, which simulates non-unitary dynamics to converge to the ground state [32]; and subspace [33] and Lanczos [34] methods, which reduce the problem's dimensionality by focusing on a subset of the Hilbert space.

Among these quantum algorithms, QPE and VQE stand out as flagship algorithms due to their theoretical rigor and experimental feasibility, respectively. QPE is theoretically exact but requires deep circuits and large qubit counts, making it best suited for future error-corrected quantum computers. VQE, on the other hand, combines shallow quantum circuits with classical optimization to minimize the energy expectation value of a parameterized quantum state (ansatz). VQE is more feasible on NISQ devices, though its accuracy depends on the choice of ansatz and optimization strategy [20].

To be implemented on quantum computers, the Hamiltonian form in Eq. (1) is transformed into the following form (the second quantization):

$$H(\mathbf{R}) = \sum_{p,q} h_{pq}(\mathbf{R}) c_p^\dagger c_q + \frac{1}{2} \sum_{p,q,r,s} h_{pqrs}(\mathbf{R}) c_p^\dagger c_q^\dagger c_r c_s. \quad (2)$$

This operation is equivalent to the basis function expansion of the wave function. Here, c_p^\dagger and c_p are the fermionic creation and annihilation operators acting on the p -th orbital. Therefore, $c_p^\dagger c_q$ is the operator to transit the state on the q -th orbital to the p -th orbital, and $c_p^\dagger c_q^\dagger c_r c_s$ is the operator to transit a pair of state $(r, s) \rightarrow (p, q)$. The one and two-electron integrals $h_{pq}(\mathbf{R})$ and $h_{pqrs}(\mathbf{R})$ in the molecular orbital basis $\phi_p(\mathbf{r})$ (yielded from the Hartree-Fock optimization procedure) depend implicitly on \mathbf{R} , which is the general nuclear coordinate associated with the fixed nuclear configuration in 3-dimensional space. These integral coefficients are calculated on the classical computer as follows:

$$h_{pq}(\mathbf{R}) = \int d\mathbf{r} \phi_p^*(\mathbf{r}) \left(-\frac{\nabla^2}{2} - \sum_m \frac{Z_m}{|\mathbf{r} - \mathbf{R}_m|} \right) \phi_q(\mathbf{r}), \quad (3)$$

$$h_{pqrs}(\mathbf{R}) = \int d\mathbf{r}_1 d\mathbf{r}_2 \frac{\phi_p^*(\mathbf{r}_1) \phi_q^*(\mathbf{r}_2) \phi_r(\mathbf{r}_2) \phi_s(\mathbf{r}_1)}{|\mathbf{r}_1 - \mathbf{r}_2|}. \quad (4)$$

The next step in implementing the Hamiltonian form in Eq. (2) in quantum circuits is to map the fermionic creation and annihilation operators to Pauli operators using methods such as the Jordan-Wigner or Bravyi-Kitaev transforms [35].

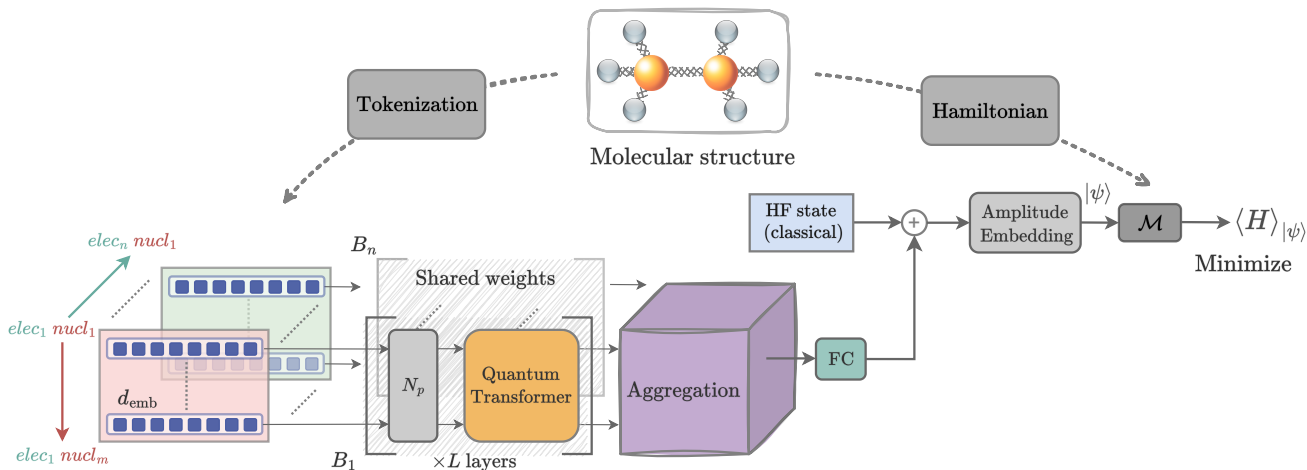


FIG. 2. Structure of Molecular Quantum Transformer (MQT). Starting with a molecule defined by atomic symbols and nuclear coordinates, the molecular Hamiltonian H is constructed in a qubit-based representation using n_q qubits. The MQT tokenizes the electronic state into an $n \times m \times d_{\text{emb}}$ feature matrix, where d_{emb} is the embedding dimension, n and m represent the number of electrons and nuclei, respectively. Tokens $elec_i$ - $nucl_j$ ($i = 1, \dots, n; j = 1, \dots, m$) are processed by blocks B_i . Each block B_i comprises L layers, including an amplification module N_p that scales features by proton number N_p and a Quantum Transformer module with shared trainable parameters. Outputs are aggregated, mapped via an FC module to match the n_q -qubit state vector, and combined with the Hartree-Fock (HF) state to produce the final state through amplitude embedding. The expectation of the Hamiltonian measured on this final state is then minimized by optimizing the model’s parameters.

B. Classical Transformer

The Transformer architecture [1] has become a crucial and widely adopted deep learning model in modern artificial intelligence. Originally developed to improve natural language processing capabilities, Transformers overcome the limitations of earlier deep learning models by effectively representing long-range dependencies and capturing complex relationships within data. The core innovation is the self-attention mechanism, which simultaneously captures correlations among all elements in a sequence, in contrast to the incremental processing of traditional models like recurrent neural networks. This parallel processing capability substantially decreases training time while also improving learning performance.

The standard architecture of Transformer is illustrated in Fig. 8 (Appendix A) with both encoder and decoder components. The encoder processes the source sequence through multiple layers, each combining multi-head self-attention with position-wise feed-forward networks. These layers are further enhanced with positional encodings, layer normalization, and residual connections to effectively capture sequential dependencies. The decoder employs masked multi-head self-attention to process the target sequence while simultaneously leveraging multi-head cross-attention to incorporate context from the encoder. The output of the decoder is refined by an additional feed-forward network and a linear layer, which generate the predictions.

In modern large language models (LLMs), the decoder-only architecture is primarily adopted. This design predicts the next token based solely on previous tokens,

making it ideal for generating coherent, context-aware text. The streamlined decoder-only structure simplifies training and scaling, enabling efficient processing of vast datasets and massive model sizes across various natural language processing tasks. Since our MQT is not developed for autoregressive language modeling, we only rely on the encoder-only Transformer. This encoder transforms the sequence of positions of molecules in different configurations into a set of contextualized representations before forwarding to the energy minimization problem. We refer to Appendix A for the detailed computational steps of the self-attention mechanism and encoder layer.

C. Molecular Quantum Transformer

We propose the Molecular Quantum Transformer (MQT) model, which replaces the VQE ansatz with a Quantum Transformer structure to determine the electron wave function that minimizes the energy associated with the Hamiltonian. The fundamental concept of the attention mechanism, described in the previous section, involves capturing correlations among all tokens simultaneously. In the context of the MQT, these tokens represent features derived from the positions and distances between atomic nuclei. As configurations change, the model adapts its features such as electron configurations based on these relationships. This adaptation is generalized through training the model across a variety of conditions. In contrast, running QPE or VQE demands independent resources for each molecular configuration, necessitating multiple models. The MQT, however, can learn

the ground-state energies for various molecules and various configurations simultaneously within a single model.

The structure of our MQT model is illustrated in Fig. 2. Given a molecular structure defined by atomic symbols and the nuclear coordinates of its constituent atoms, we construct the molecular Hamiltonian H in a qubit-based representation using n_q qubits as a preprocessing step. Here, we utilize the PennyLane molecules dataset [36] and its built-in functions [37] to generate the corresponding molecular Hamiltonians. The MQT begins with a tokenization module that creates input tokens $elec_i-nucl_j$ ($i = 1, \dots, n; j = 1, \dots, m$), representing the electronic state as an $n \times m$ two-dimensional array of d_{emb} -dimensional features. Here, d_{emb} is the embedding dimension, n and m denote the number of electrons and nuclei, respectively, resulting in an $n \times m \times d_{\text{emb}}$ feature matrix. For each electron index i , the m tokens $elec_i-nucl_j$ ($j = 1, \dots, m$) are processed by a block B_i , which consists of L layers. Each layer includes an amplification module N_p and a Quantum Transformer module. The amplification module N_p scales the feature values by the proton number N_p to reflect the differences among nuclear species before passing them to the Quantum Transformer module. The Quantum Transformer module contains trainable parameters, which are shared across all blocks B_1, \dots, B_n . The outputs of all Quantum Transformer modules are combined into a single feature representation via an aggregation module. A fully connected (FC) module then maps this aggregated feature into a vector with the same dimensionality as the n_q -qubit state vector. This transformed vector is subsequently added to the Hartree-Fock (HF) state vector, and the resulting representation is used to generate the final electronic state through an amplitude embedding module. The expectation value of the Hamiltonian H is computed from this amplitude-embedded state via a measurement process. This expectation value is minimized by optimizing the trainable parameters in the Quantum Transformer, aggregation, and FC modules.

1. Tokenization

Figure 3(a) provides a detailed description of the tokenization module and Quantum Transformer module. Following a token preparation approach similar to that in Ref. [38], each d_{emb} -dimensional feature input vector \mathbf{x} in the token matrix is derived from a vector concatenating the relative positions of electrons to each nucleus ($p_{\text{en}}^{\text{in}}$) and their initial distances ($r_{\text{en}}^{\text{in}}$), processed through a fully-connected (FC) layer with trainable weights W_{en} . The computational steps to obtain $p_{\text{en}}^{\text{in}}$ and $r_{\text{en}}^{\text{in}}$ are outlined as follows:

- *Input*: The input consists of the positions of individual atoms (nuclear coordinates) and electron identifiers (atomic orbital assignments). For example, in BeH_2 , the 3D coordinates of the Hydrogen (H) atoms are symmetrically positioned along the

z -axis at $(0, 0, -2.5)$ and $(0, 0, 2.5)$, with the Beryllium (Be) atom at the origin $(0, 0, 0)$. The nucleus position is an $m \times 3$ matrix with $m = 3$, where the first and last rows correspond to the two H atoms. Electron identifiers are assigned as follows: [1] (1s) for the first H, [1] (1s), [2] (1s), [3] (2s), and [4] (2s) for Be, and [1] (1s) for the second H.

- *Embedding (1)*: Each electron identifier is converted into a one-hot vector of dimension equal to the maximum identifier (4 in the BeH_2 example). Thus, all n electron identifiers are represented as $n \times 4$ binary matrix. This matrix is then multiplied by a 4×3 trainable weight matrix to produce an $n \times 3$ matrix of electron relative positions. These positions are relative to their respective atoms, and the trainable weights ensure that electron positions adapt to changes in the molecular structure.
- *Adder (2)*: The absolute position of each electron is computed by adding its relative position to the position of its associated atom, resulting in an $n \times 3$ matrix.
- *Subtraction (3)*: The relative positions between all electrons and all nuclei are calculated. For each nucleus, an $n \times 3$ matrix is obtained by subtracting the absolute positions of all electrons from that nucleus's position, yielding an output matrix $p_{\text{en}}^{\text{in}}$ of shape $n \times m \times 3$.
- *Concatenation (4)*: The relative distance matrix $r_{\text{en}}^{\text{in}}$, with shape $n \times m \times 1$, is derived from $p_{\text{en}}^{\text{in}}$ where each element in $r_{\text{en}}^{\text{in}}$ is the Euclidean norm of each position vector. Concatenating $p_{\text{en}}^{\text{in}}$ with $r_{\text{en}}^{\text{in}}$ produces an $n \times m \times 4$ matrix.

2. Quantum Transformer

The architecture of the Quantum Transformer component in MQT is depicted in the lower panel of Fig. 3(a), consisting of L repeated layers. In each layer, the input features, derived from classical representation of the molecule are processed through the arccos, tanh, and amplification N_p modules. For each electron, this generates an $m \times d_{\text{emb}}$ features matrix corresponding to m tokens \mathbf{x}_j . Each d_{emb} -dimensional feature vector of token \mathbf{x}_j is embedded into a quantum state $|\psi_{j,0}\rangle$ via an angle embedding layer using d_{emb} qubits. Query, Key, and Value transformations, implemented with quantum ansatzes, are then applied to update the states $|\psi_{j,k-1}\rangle \rightarrow |\psi_{j,k}\rangle$ ($k = 1, \dots, m$) through a quantum self-attention mechanism. The final quantum state $|\psi_{j,m}\rangle$ is measured in the computational basis and converted back into classical features of dimension $m \times d_{\text{emb}}$, yielding an $n \times m \times d_{\text{emb}}$ feature matrix for n blocks of n electrons. These features are added to the input features via a residual connection and normalization to produce the input for the next layer.

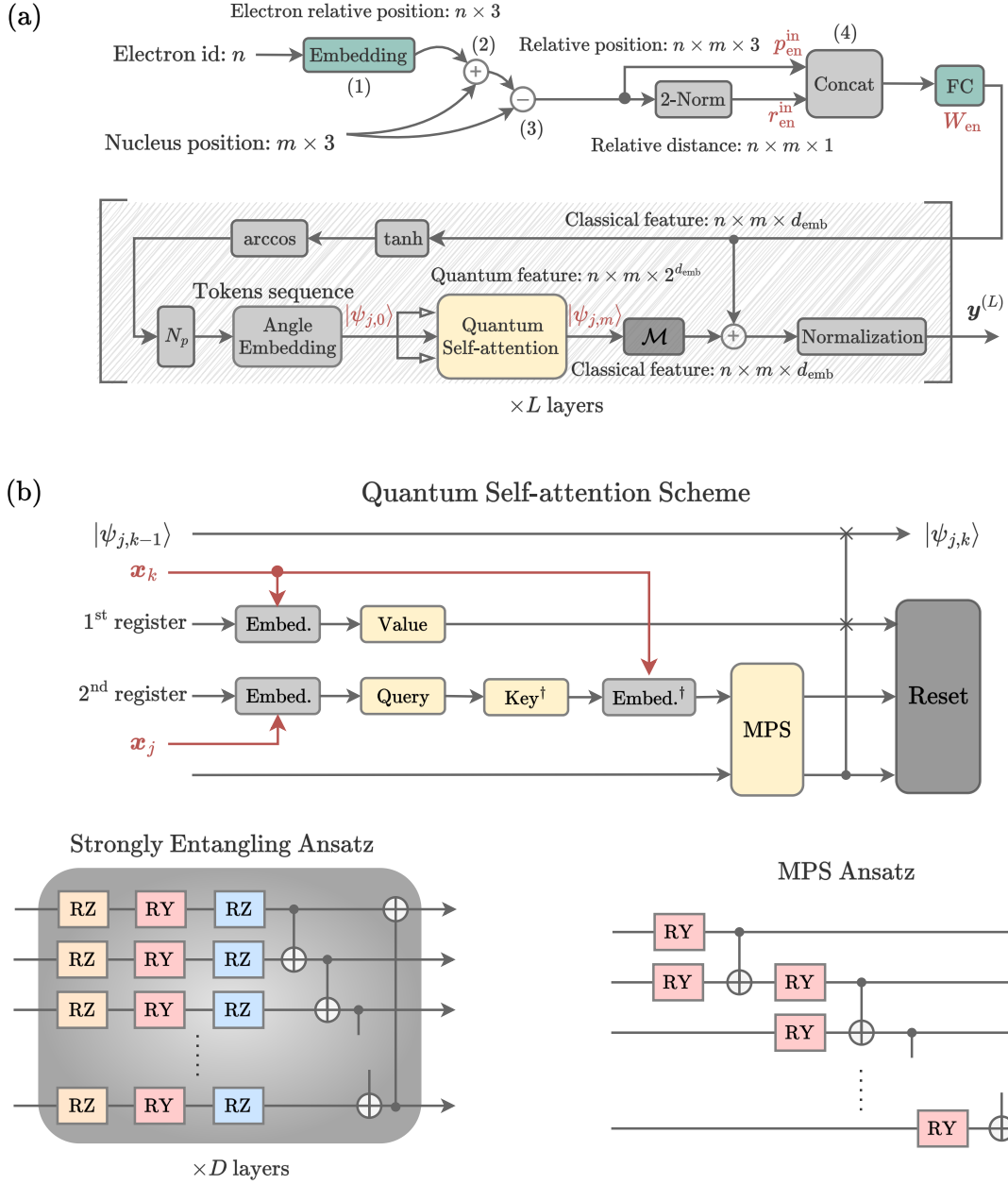


FIG. 3. (a) Tokenization and Quantum Transformer module in the MQT. (Upper panel) Each token vector is derived from concatenated relative electron-nucleus positions (p_{en}^{in}) and distances (r_{en}^{in}), processed through a fully-connected (FC) layer with trainable weights W_{en} . (Lower panel) The Quantum Transformer comprises L repeated layers, processing input features with \arccos , \tanh , and amplification N_p modules to generate an $m \times d_{emb}$ features matrix of m tokens \mathbf{x}_j for each electron. Each d_{emb} -dimensional feature vector of token \mathbf{x}_j is embedded into a quantum state $|\psi_{j,0}\rangle$ via an angle embedding layer using d_{emb} qubits, updated via Query, Key, and Value transformations ($|\psi_{j,k-1}\rangle \rightarrow |\psi_{j,k}\rangle$ ($k = 1, \dots, m$)) using a quantum self-attention mechanism. The measurement in the final state $|\psi_{j,m}\rangle$ yields an $n \times m \times d_{emb}$ feature matrix for n blocks of n electrons. These features are added to the input features via a residual connection and normalization to produce the input for the next layer. (b) Quantum self-attention update ($|\psi_{j,k-1}\rangle \rightarrow |\psi_{j,k}\rangle$). For token \mathbf{x}_j , angle embedding with R_Y rotation gate (Embed.) uses a second auxiliary token register, followed by Query and the adjoint Key transformations, which are constructed with a single layer of strongly entangling (StrEnt) ansatz. Then the adjoint matrix of the angle embedding (Embed. †) for the token \mathbf{x}_k is applied to compute the Hadamard product of the Query and Key. This product is then transformed into a 1-qubit attention representation using a 2-bond matrix product state (MPS) ansatz implemented with an additional ancilla qubit. Value transformation for \mathbf{x}_k (first auxiliary token register, Embed. and a six-layer StrEnt ansatz) and a controlled SWAP gate complete the update. The StrEnt and MPS ansatzes are depicted in the lower panel with the trainable rotation gates.

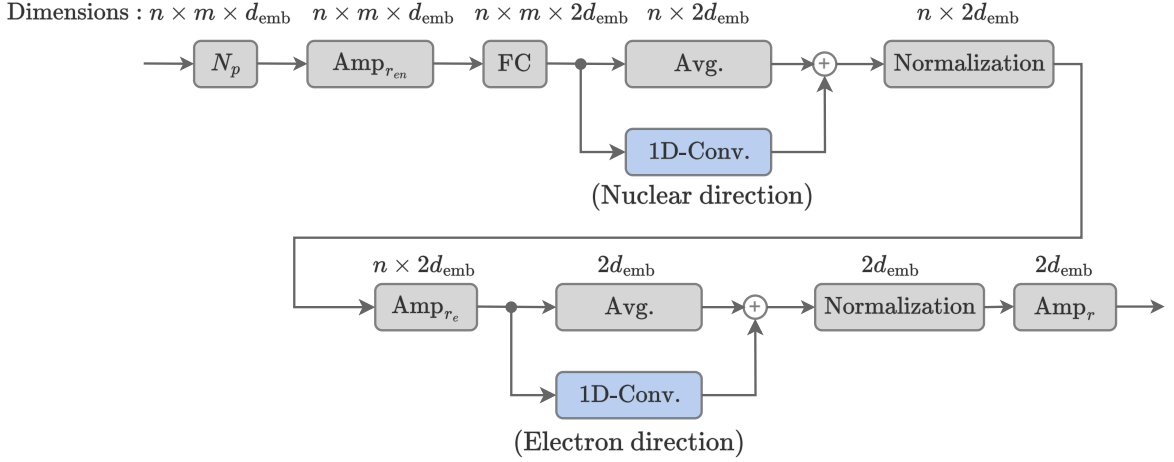


FIG. 4. The aggregation module transforming the Quantum Transformer output matrix $\mathbf{y}^{(L)}$ ($n \times m \times d_{\text{emb}}$) into an $2d_{\text{emb}}$ -dimensional feature vector. The process applies amplification modules N_p and $\text{Amp}_{r_{\text{en}}}$, followed by an FC module yielding $n \times m \times (2d_{\text{emb}})$ features. These are processed along the nuclear dimension direction by Avg. and 1D-Conv. modules, summed into $n \times (2d_{\text{emb}})$ features, and adjusted by Amp_{r_e} using r_e (averaged value of r_{en}). Further Avg. and 1D-Conv. modules along the electron dimension direction, followed by a normalization and Amp_r , produce the final vector.

The detailed of the update $|\psi_{j,k-1}\rangle \rightarrow |\psi_{j,k}\rangle$ is shown in Fig. 3(b). For an input token \mathbf{x}_j , angle embedding is performed using a R_Y rotation gate (Embed.) on a second auxiliary token register. This is followed by a Query transformation and the adjoint of Key transformation, both constructed with a single layer of strongly entangling (StrEnt) ansatz. Then the adjoint matrix of the angle embedding (Embed.[†]) for token \mathbf{x}_k is applied to compute the Hadamard product of the Query and Key, which resembles the single-head attention. This product is then transformed into a 1-qubit attention representation using a 2-bond matrix product state (MPS) ansatz implemented with trainable R_Y and an additional ancilla qubit. Next, a Value transformation for \mathbf{x}_k is applied using the first auxiliary token register, involving the angle embedding (Embed.) and a six-layer StrEnt ansatz. Finally, a controlled SWAP gate updates the features based on the attention representation.

3. Aggregation

The outputs of all Quantum Transformer modules are summarized into a feature matrix $\mathbf{y}^{(L)}$ of dimension $n \times m \times d_{\text{emb}}$, which is then transformed into a 16 -dimensional feature vector via an aggregation module. We illustrate the aggregation module in Fig. 4. Initially, the amplification modules N_p and $\text{Amp}_{r_{\text{en}}}$ are applied to $\mathbf{y}^{(L)}$ without altering its dimension. Each element y_{ijk} ($1 \leq i \leq n$, $1 \leq j \leq m$, $1 \leq k \leq d_{\text{emb}}$) in $\mathbf{y}^{(L)}$ is transformed as:

$$y_{ijk} \rightarrow e^{-r_{\text{en}}(i,j,0)} N_p y_{ijk}, \quad (5)$$

where N_p is the proton number, r_{en} is the $n \times m \times 1$ electron-nucleus relative distance matrix with elements $r_{\text{en}}(i, j, 0)$ ($1 \leq i \leq n$, $1 \leq j \leq m$). The relative distance r_{en} is updated from the initial distance $r_{\text{en}}^{\text{in}}$ using the attention scheme through the following inversion:

$$[p_{\text{en}}^{\text{out}}, r_{\text{en}}^{\text{out}}] = (W_{\text{en}}^{\text{T}} \times W_{\text{en}})^{-1} \times W_{\text{en}}^{\text{T}} \times \mathbf{y}^{(L)}, \quad (6)$$

$$r_{\text{en}} = \text{std}(r_{\text{en}}^{\text{in}}) \times \frac{r_{\text{en}}^{\text{out}} - \text{mean}(r_{\text{en}}^{\text{out}})}{\text{std}(r_{\text{en}}^{\text{out}})} + \text{mean}(r_{\text{en}}^{\text{in}}), \quad (7)$$

where $\text{mean}(A)$ and $\text{std}(A)$ denote for the scalar mean and standard deviation of all elements in matrix A , and $r_{\text{en}}^{\text{in}}$ and $r_{\text{en}}^{\text{out}}$ share the $n \times m \times 1$ dimension. Here, \times , $+$, $-$ are broadcast operators applied element-wise to $r_{\text{en}}^{\text{out}}$.

The output of $\text{Amp}_{r_{\text{en}}}$ with dimension $n \times m \times d_{\text{emb}}$ is processed by an FC module with trainable weights to obtain features of dimension $n \times m \times (2d_{\text{emb}})$. These features are then separately processed along the nuclear dimension direction (second axis) by an averaging (Avg.) module and a one-dimensional convolutional (1D-Conv.) module (kernel size 2, stride 2), and the results are summed to produce an $n \times (2d_{\text{emb}})$ feature matrix. This matrix is normalized and adjusted by the amplification module Amp_{r_e} , where r_e (dimension n) is the average r_{en} across its second dimension. The amplification module Amp_{r_e} multiplies each element at the index (i, k) ($1 \leq i \leq n$, $1 \leq k \leq 2d_{\text{emb}}$) of the feature matrix to $e^{-r_e(i)}$ where $r_e(i)$ is the i -element in r_e . The output is then separately processed by Avg. and 1D-Conv. modules along the electron dimension direction (the first axis), summed to form a $2d_{\text{emb}}$ -dimensional feature vector, and further normalized and amplified by Amp_r . Here r is the scalar average of r_e , and each element of the vector is multiplied by e^{-r} .

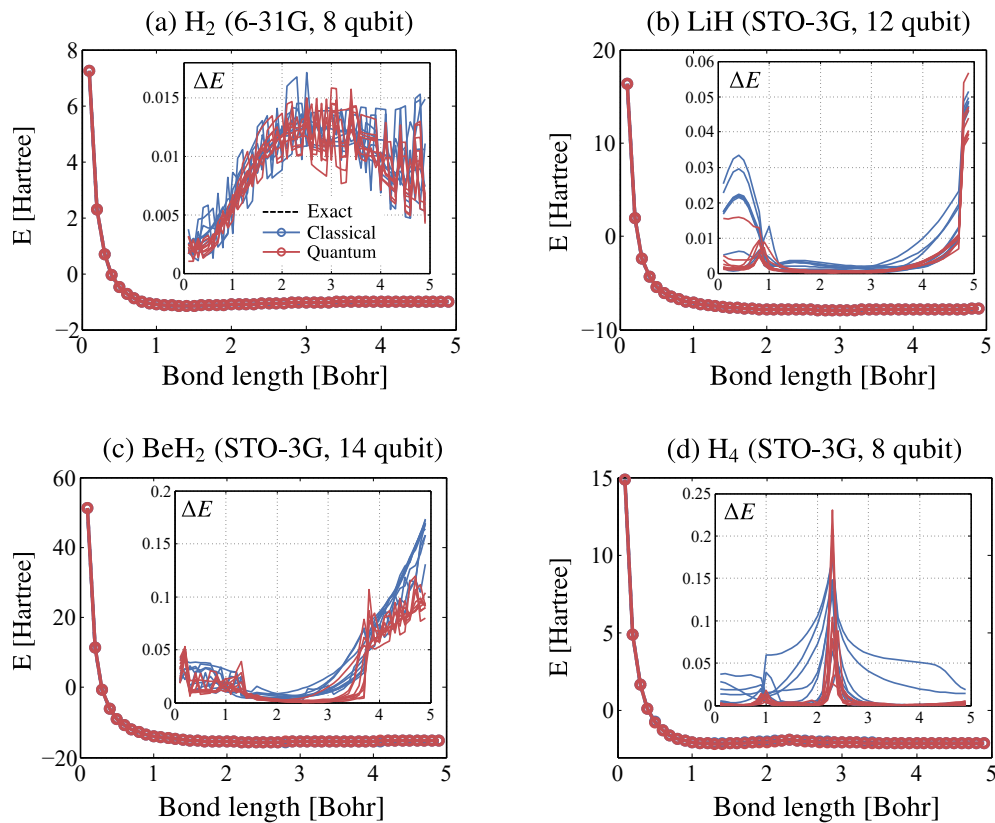


FIG. 5. Potential energy curves and estimation errors (ΔE) in the inset figures for varying interatomic bond lengths in (a) H_2 (b) LiH , (c) BeH_2 , and (d) H_4 molecules using the quantum (red lines) and classical (blue lines) Transformers.

III. RESULTS

In the following numerical experiments, we apply MQT to estimate the potential energy curves (PEC) of molecular Hamiltonian for H_2 , LiH , BeH_2 , and H_4 . For the second quantization of the Hamiltonians, we employ the Bravyi-Kitaev mapping for H_2 (8 qubits), LiH (12 qubits), and BeH_2 (14 qubits), and the Jordan-Wigner transformation for H_4 (8 qubits). The 6-31G basis set is used for H_2 , while STO-3G basis set is applied to the other molecules.

We first evaluate MQT in a plain training scenario, where it is trained and tested on data from the same molecule. Subsequently, we investigate the pretraining effect by training MQT on H_2 , BeH_2 , and H_4 , followed by fine-tuning on a different molecule (LiH). We set the embedding dimension $d_{\text{emb}} = 8$ as the default setting for these experiments.

A. Estimating the potential energy curve with plain training

In plain training, the token matrix is generated in each iteration from a configuration with a random bond length sampled from (0.0, 5.0) [Bohr]. After training, the poten-

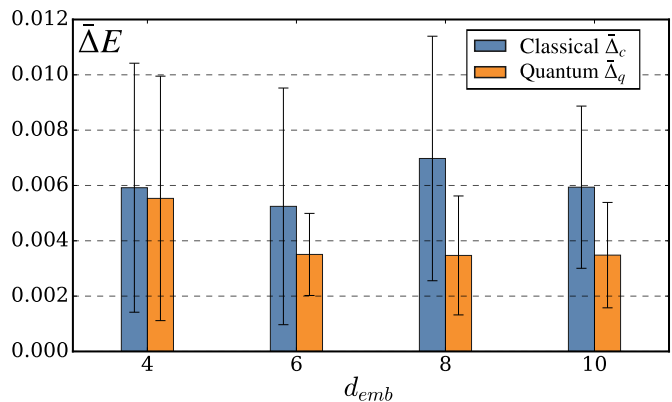


FIG. 6. Bar plot comparing the average ground-state energy estimation error of LiH over potential energy curves between the classical Transformer ($\overline{\Delta}_c$) and MQT ($\overline{\Delta}_q$) as a function of the token embedding dimension d_{emb} (4, 6, 8, 10). Error bars represent standard deviations. Teal-blue bars indicate classical results, while orange bars indicate quantum results, highlighting MQT's consistently lower errors across d_{emb} .

tial energy curves are estimated for bond lengths ranging from 0.1 to 4.9 [Bohr] in 0.1 [Bohr] increments using the trained model. We use $L = 6$ layers of Quantum Transformer module in each processing block B_i as shown in Fig. 2. We compare the performance of MQT

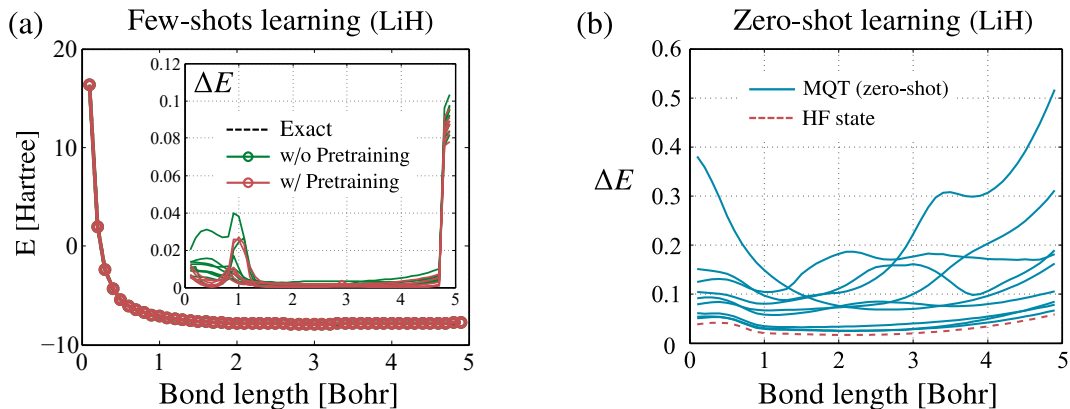


FIG. 7. The few-shot and zero-shot learning of MQT for LiH potential energy curves. (a) Potential energy curves and estimation errors (ΔE) in the inset show MQT trained on LiH with a few data points, comparing pretraining on H_2 , BeH_2 , and H_4 (red lines) versus no pretraining (green lines) across varying bond lengths. (b) Zero-shot MQT, pretrained on H_2 , BeH_2 , and H_4 but not fine-tuned on LiH, with the estimation errors from nine trials compared to the errors by the Hartree-Fock (HF) state.

against a classical Transformer implementation replacing the Quantum Transformer module in Fig. 2. To align with the settings of MQT, we consider the classical Transformer with d_{emb} embedding dimensions, $4 \times d_{\text{emb}}$ hidden dimensions (see Appendix A for the definition of the hidden dimension), and a single-head attention. We use AdamW optimizer with a weight decay rate of 0.001. The learning rate is set to 0.008 for the classical Transformer with H_2 ; and 0.004 for other cases. In the optimization, we employ the method in Ref. [39] to run four processes in parallel on a single GPU, with each process performing 2500 iterations, for a total of 10^4 iterations.

Metric	H_2	LiH	BeH_2	H_4
$\bar{\Delta}_c$	9.3e-3	7.0e-3	3.3e-2	1.9e-2
$\bar{\Delta}_q$	8.9e-3	3.9e-3	2.7e-2	0.5e-2

TABLE I. Average ground-state energy estimation error by classical Transformer ($\bar{\Delta}_c$) and MQT ($\bar{\Delta}_q$)

Figure 5 compares the energy estimations of the MQT and classical Transformer against the theoretically calculated ground-state energies of the Hamiltonians for each molecule. The inset figures show the estimation errors relative to the true ground-state energy, with each line representing one of nine trials. MQT exhibits lower estimation errors than the classical Transformer for (b) LiH, (c) BeH_2 , and (d) H_4 . For (a) H_2 , the estimation errors of MQT are nearly identical to those of the classical Transformer (note the differing y-axis scales across plots). The average estimation errors across all tested bond lengths for the classical Transformer ($\bar{\Delta}_c$) and MQT ($\bar{\Delta}_q$) are summarized in Tab. I. These results suggest that MQT performs comparably to the classical Transformer for H_2 but outperforms it for other molecules, reducing the average estimation error by 44% in LiH, 18% in BeH_2 , and 74% in H_4 compared to the classical Transformer. In

Fig. 6, we further compare $\bar{\Delta}_c$ and $\bar{\Delta}_q$ of LiH for different embedding dimension $d_{\text{emb}} \in \{4, 6, 8, 10\}$. MQT shows lower estimation error consistency with all d_{emb} and achieves the saturated value when $d_{\text{emb}} \geq 6$. These findings highlight the potential benefits of incorporating quantum structures into the Transformer framework.

B. Estimating the potential energy curve with pretraining

The MQT model, pretrained on multiple molecules (H_2 , BeH_2 , H_4) is fine-tuned with a small number of data points for LiH. Here, a few-shot learning approach is performed to estimate the potential energy curve of LiH.

During fine-tuning, the training mirrors the setting in the pretraining stage, employing the AdamW optimizer with a weight decay of 10^{-3} and a learning rate of 4×10^{-3} . The training data for LiH consisted of five randomly selected bond lengths: $\{0.5, 1.5, 2.5, 3.5, 4.5\}$ [Bohr]. The method in Ref. [39] is employed to run four processes in parallel on a single GPU, with each process performing 500 iterations, for a total of 2000 iterations for fine-tuning. After the fine-tuning, potential energy curves are estimated for bond lengths from 0.1 to 4.9 Bohr in 0.1 Bohr increments. Figure 7(a) depicts the average estimated energy curves for pretraining and fine-tuning (red lines, labeled “w/ Pretraining”) and fine-tuning only (green lines, labeled “w/o Pretraining”), with an inset displaying error curves across nine trials. The pretrained model yields more accurate estimations in few-shot learning compared to only using fine-tuning, as indicated by reducing nearly 19% of error to the theoretical values from 7.6×10^{-3} (“w/o Pretraining”) the 6.2×10^{-3} (“w/ Pretraining”).

To further examine the effect of few-shot learning, we evaluate the zero-shot learning, where the pre-trained MQT is tested on LiH without fine-tuning. As shown in

Fig. 7(b), the estimation error of MQT significantly exceeds that of the Hartree-Fock state, indicating that zero-shot learning is inadequate. At least a few data points (few-shot learning) are necessary during fine-tuning to enhance estimation accuracy.

IV. CONCLUSION AND DISCUSSION

We propose the MQT model, which leverages the quantum attention mechanism to revolutionize the calculation of ground-state energies. The key contribution is that MQT can be adapted to train on multiple molecules and multiple configurations without altering the model structure. This approach can open new avenues in quantum chemistry and materials science, where an accurate understanding of ground-state energies is crucial, but running routines such as VQE and QPE independently for each molecule and configuration requires high cost.

In our numerical experiment, we evaluated the performance of MQT in estimating potential energy curves for H_2 , LiH , BeH_2 , and H_4 , benchmarking it against a classical Transformer. MQT consistently outperformed the classical model in estimation accuracy. We also investigated pretraining MQT on multiple molecules (H_2 , BeH_2 , and H_4) and evaluated the few-shot learning capability on LiH . Results showed that pretraining modestly improved accuracy for the LiH potential energy curve compared to an untrained model. In scenarios with small molecules and readily available training data, pretraining MQT can significantly reduce the number of quantum circuit runs required for larger and more complex molecular systems. To maximize this pretraining advantage, designing suitable pretraining datasets for specific molecules is crucial. Ideally, with sufficient high-quality pretraining data, MQT could estimate the potential energy surface of a given molecule without a few-shot learning on that molecule.

Scaling MQT to larger molecules requires addressing several limitations. A primary bottleneck is the output quantum state representation via amplitude embedding, where direct state preparation is challenging due to complexity scaling exponentially with the number of qubits n_q . The qRAM [9] scheme could reduce this complexity to near-linear in n_q , but fault-tolerant qRAM remains an engineering challenge. Even with efficient qRAM, preparing the state vector on a classical computer prior to amplitude embedding demands memory that grows exponentially with n_q , hindering scalability. Inspired by the divide-and-conquer approach in VQE [40], we can concatenate MQTs to enable the application to large systems with strong intrasubsystem and weak inter-subsystem interactions on small-scale quantum computers. Thus, our method still offers a promising framework for tackling practically significant, large-scale problems in quantum chemistry.

In this paper, MQT is developed to exploit the classical representation of a molecule and its associated Hamilto-

nian, enabling efficient computation of electronic properties within a quantum framework. This approach necessitates an embedding procedure to transform the classical representation into quantum features suitable for processing on quantum hardware. As a future direction, MQT could be extended to integrate directly with quantum-native representations of molecular states, bypassing classical intermediaries. For instance, incorporating the noisy ground state estimates obtained from VQE or the intermediate eigenstate data from the QPE process could enrich MQT with detailed quantum information about the ground state and low-lying excited states. Such an integration promises to enhance the accuracy of MQT by leveraging the intrinsic quantum correlations captured in these states, which are often inaccessible to classical methods like DFT or CI. Furthermore, this approach could be combined with advanced quantum techniques, such as quantum denoising mechanisms [41] to mitigate errors from NISQ devices, or quantum curriculum learning algorithms [42] to optimize the training of quantum circuits. These enhancements could position MQT as a versatile tool for tackling the molecular electronic problem, potentially outperforming traditional hybrid quantum-classical workflows in both precision and scalability.

ACKNOWLEDGMENTS

The authors acknowledge Shintaro Sato, Koki Chinzei, and Nasa Matsumoto for their fruitful discussions. Special thanks are extended to Koki Chinzei for his valuable comments on the design of the MQT model.

Appendix A: Classical Transformer

The standard architecture of Transformer is illustrated in Fig. 8 with both encoder and decoder components. The encoder processes the source sequence through multiple layers, each combining multi-head self-attention with position-wise feed-forward networks. These layers are further enhanced with positional encodings, layer normalization, and residual connections (the arrows bypassing the main components, such as the attention and feed-forward layers) and to effectively capture sequential dependencies. The decoder employs masked multi-head self-attention to process the target sequence while simultaneously leveraging multi-head cross-attention to incorporate context from the encoder. The output of the decoder is refined by an additional feed-forward network and a linear layer, which generate the predictions. In our MQT, we only rely on the encoder-only Transformer to transform the position sequence of molecules in different configurations into a set of rich and contextualized representations. Therefore, in the remainder of this section, we focus on detailing the implementation of encoder-only Transformer architectures.

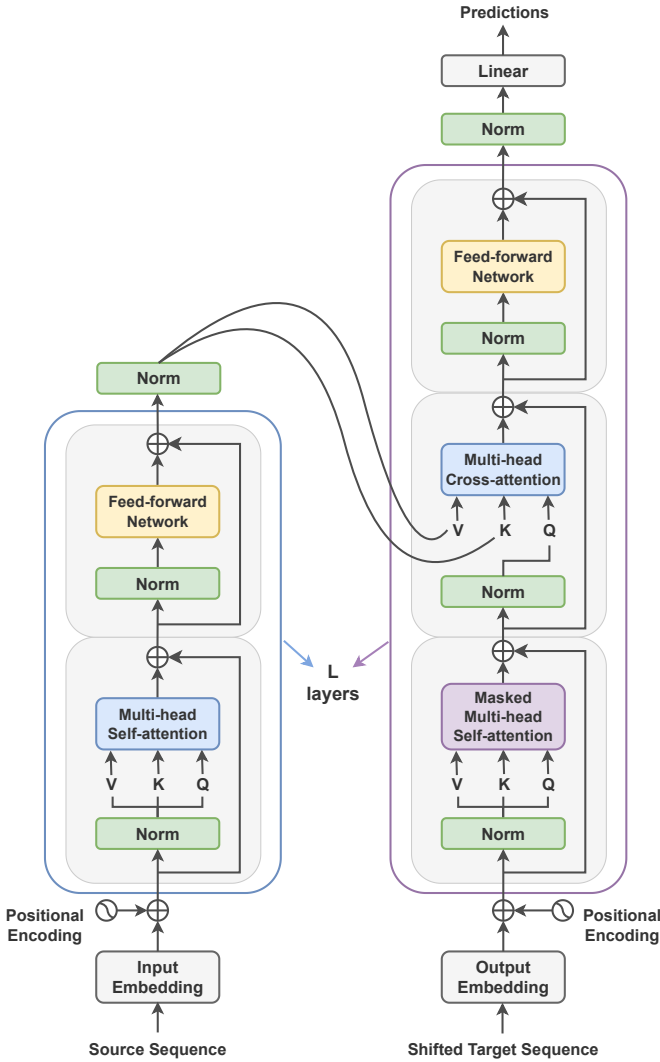


FIG. 8. Standard architecture of classical Transformer with an encoder (left) and a decoder (right). The encoder processes the source sequence through layers that combine multi-head self-attention and position-wise feed-forward networks, enhanced with positional encodings, layer normalization, and residual (bypass) connections. The decoder applies masked multi-head self-attention to the target sequence and cross-attention to integrate encoder context, with its output refined by a feed-forward network and a linear layer to generate predictions. The figure has been recreated to clearly detail the sequential operations originally shown in Ref. [1] and modified in Ref. [43].

The encoder-only Transformer operates by:

1. Embedding the input tokens and adding positional encodings.
2. Passing these embeddings through multiple identical layers.
3. In each layer, applying multi-head self-attention to capture relationships between tokens, followed by

a position-wise feed-forward network to transform the representations.

4. Using residual connections and layer normalization to maintain gradient flow and stabilize training.

This design enables efficient and parallelizable processing of sequences while capturing complex dependencies within the data.

1. Tokenization and Input Representation

Transformers employ tokenization to convert sequential data into discrete units. Tokenization breaks a sequence into smaller units called *tokens*. Given an input sequence of tokens x_1, x_2, \dots, x_n , each token is first mapped into a continuous embedding vector. Let the embedding function be $e(\cdot)$ so that:

$$E = \begin{bmatrix} e(x_1) \\ e(x_2) \\ \vdots \\ e(x_n) \end{bmatrix} \in \mathbb{R}^{n \times d_{\text{emb}}}, \quad (\text{A1})$$

where d_{emb} is the embedding dimension. Transformers do not inherently encode token order. Instead, a positional encoding $P \in \mathbb{R}^{n \times d_{\text{emb}}}$ is added to the embeddings as $Z^{(0)} = E + P$.

2. Self-attention and Encoder Layer

The encoder is composed of L identical layers. Each layer has two main sub-layers: multi-head self-attention and a position-wise feed-forward network, with residual connections and layer normalization applied around each sub-layer. Self-attention is the core component of the Transformer architecture with the capability to model token interdependencies. It allows each token in the sequence to dynamically incorporate information from all other tokens by computing inner-product-based attention scores. This operation, known as *scaled dot-product attention*, produces attention matrices that quantify the relevance of each token relative to the others, effectively capturing complex contextual relationships across the entire sequence. The Transformer also incorporates the multi-head attention mechanism, which extends self-attention by computing multiple attention matrices in parallel. Each attention head is trained to capture different relationships between tokens in the sequence, allowing the model to process information from multiple embedding subspaces simultaneously. Typically, Transformer uses high-dimensional embeddings, which are divided across several attention heads.

For the l -th layer ($l = 1, 2, \dots, L$) of the encoder, the input is $Z^{(l-1)}$ and the output is $Z^{(l)} = \text{en}_l(Z^{(l-1)})$. The

detailed computational steps of the l layer are described as follows:

- 1. Layer normalization and projections:** The input $Z^{(l-1)}$ is normalized across the features for each individual data point to $\hat{Z}^{(l-1)}$ and then linearly projected to form queries Q , keys K , and values V . For each attention head i ($i = 1, \dots, h$), we have:

$$Q_i = \hat{Z}^{(l-1)} W_i^Q, \quad K_i = \hat{Z}^{(l-1)} W_i^K, \quad V_i = \hat{Z}^{(l-1)} W_i^V, \quad (\text{A2})$$

where trainable parameters $W_i^Q, W_i^K, W_i^V \in \mathbb{R}^{d_{\text{emb}} \times d_k}$ and typically $d_k = \frac{d_{\text{emb}}}{h}$.

- 2. Scaled dot-product attention:** For each head, the attention output is computed as:

$$\text{head}_i = \text{Attention}(Q_i, K_i, V_i) = \text{softmax}\left(\frac{Q_i K_i^T}{\sqrt{d_k}}\right) V_i. \quad (\text{A3})$$

- 3. Concatenation and projection:** The outputs of all heads are concatenated and projected:

$$\text{MultiHead}(Z^{(l-1)}) = \text{Concat}(\text{head}_1, \dots, \text{head}_h) W^O, \quad (\text{A4})$$

where trainable parameters $W^O \in \mathbb{R}^{hd_k \times d_{\text{emb}}}$.

- 4. Residual connection and normalization:** The output of the multi-head attention is added to the original input $Z^{(l-1)}$ (residual connection), and then normalized:

$$\hat{Z}^{(l)} = \text{LayerNorm}\left(Z^{(l-1)} + \text{MultiHead}(Z^{(l-1)})\right). \quad (\text{A5})$$

5. Position-wise feed-forward network (FFN):

The normalized output $\hat{Z}^{(l)}$ is processed by a two-layer feed-forward network applied independently to each position:

$$\text{FFN}(\hat{Z}^{(l)}) = \sigma\left(\hat{Z}^{(l)} W_1 + b_1\right) W_2 + b_2, \quad (\text{A6})$$

where trainable parameters $W_1 \in \mathbb{R}^{d_{\text{emb}} \times d_{\text{ff}}}$, $b_1 \in \mathbb{R}^{d_{\text{ff}}}$, $W_2 \in \mathbb{R}^{d_{\text{ff}} \times d_{\text{emb}}}$, $b_2 \in \mathbb{R}^{d_{\text{emb}}}$, and $\sigma(x)$ is an activation function such as $\tanh(x)$ and $\text{ReLU}(x) = \max(0, x)$. Here, d_{ff} is the hidden dimension of the FFN, typically larger than d_{emb} .

6. Residual connection:

$$Z^{(l)} = \text{LayerNorm}\left(\hat{Z}^{(l)} + \text{FFN}(\hat{Z}^{(l)})\right). \quad (\text{A7})$$

After processing through L identical layers, the final encoder output is:

$$Z^{(L)} = \text{LayerNorm}\left(\text{en}_L\left(\dots \text{en}_1\left(Z^{(0)}\right)\dots\right)\right). \quad (\text{A8})$$

This output $Z^{(L)}$ is a set of context-rich representations for the input tokens, encapsulating both local and global dependencies, and can be used for various downstream tasks such as classification, regression, or serving as input to a decoder in sequence-to-sequence models.

-
- [1] A. Vaswani, N. Shazeer, N. Parmar, J. Uszkoreit, L. Jones, A. N. Gomez, L. u. Kaiser, and I. Polosukhin, in *Advances in Neural Information Processing Systems*, Vol. 30 (Curran Associates, Inc., 2017).
- [2] J. Biamonte, P. Wittek, N. Pancotti, P. Rebentrost, N. Wiebe, and S. Lloyd, *Nature* **549**, 195 (2017).
- [3] M. Schuld and F. Petruccione, *Machine Learning with Quantum Computers* (Springer International Publishing, 2021).
- [4] V. Havlíček, A. D. Córcoles, K. Temme, A. W. Harrow, A. Kandala, J. M. Chow, and J. M. Gambetta, *Nature* **567**, 209 (2019).
- [5] M. Schuld and N. Killoran, *Phys. Rev. Lett.* **122**, 040504 (2019).
- [6] R. D. Sipio, J.-H. Huang, S. Y.-C. Chen, S. Mangini, and M. Worring, *The dawn of quantum natural language processing* (2021).
- [7] G. Li, X. Zhao, and X. Wang, *Sci. China Inf. Sci.* **67**, 142501 (2024).
- [8] C. Xue, Z.-Y. Chen, X.-N. Zhuang, Y.-J. Wang, T.-P. Sun, J.-C. Wang, H.-Y. Liu, Y.-C. Wu, Z.-L. Wang, and G.-P. Guo, arXiv [10.48550/arxiv.2402.18940](https://arxiv.org/abs/10.48550/arxiv.2402.18940) (2024).
- [9] V. Giovannetti, S. Lloyd, and L. Maccone, *Phys. Rev. Lett.* **100**, 160501 (2008).
- [10] E. A. Cherrat, I. Kerenidis, N. Mathur, J. Landman, M. Strahm, and Y. Y. Li, *Quantum* **8**, 1265 (2024).
- [11] A. M. Smaldone, Y. Shee, G. W. Kyro, M. H. Farag, Z. Chandani, E. Kyoseva, and V. S. Batista, arXiv [10.48550/arxiv.2502.19214](https://arxiv.org/abs/10.48550/arxiv.2502.19214) (2025).
- [12] J. Zheng, Q. Gao, and Z. Miao, in *2023 IEEE International Conference on Systems, Man, and Cybernetics (SMC)* (IEEE, 2023) p. 1058–1063.
- [13] E. N. Evans, M. Cook, Z. P. Bradshaw, and M. L. LaBorde, arXiv [10.48550/arxiv.2403.14753](https://arxiv.org/abs/10.48550/arxiv.2403.14753) (2025).
- [14] *Nat. Mach. Intell.* **5**, 813–813 (2023).
- [15] A. Peruzzo, J. McClean, P. Shadbolt, M.-H. Yung, X.-Q. Zhou, P. J. Love, A. Aspuru-Guzik, and J. L. O’Brien, *Nat. Commun.* **5**, 4213 (2014).
- [16] A. Kandala, A. Mezzacapo, K. Temme, M. Takita, M. Brink, J. M. Chow, and J. M. Gambetta, *Nature* **549**,

- 242 (2017).
- [17] A. Y. Kitaev, *Electron. Colloquium Comput. Complex.* **TR96** (1995).
- [18] M. A. Nielsen and I. L. Chuang, *Quantum Computation and Quantum Information*, 10th ed. (Cambridge University Press, 2010).
- [19] J. Lee, D. W. Berry, C. Gidney, W. J. Huggins, J. R. McClean, N. Wiebe, and R. Babbush, *PRX Quantum* **2**, 030305 (2021).
- [20] J. Tilly, H. Chen, S. Cao, D. Picozzi, K. Setia, Y. Li, E. Grant, L. Wossnig, I. Rungger, G. H. Booth, and J. Tennyson, *Physics Reports* **986**, 1 (2022), the Variational Quantum Eigensolver: a review of methods and best practices.
- [21] J. F. Gonthier, M. D. Radin, C. Buda, E. J. Duskocil, C. M. Abuan, and J. Romero, *Phys. Rev. Res.* **4**, 033154 (2022).
- [22] A. Cervera-Lierta, J. S. Kottmann, and A. Aspuru-Guzik, *PRX Quantum* **2**, 020329 (2021).
- [23] J. Ceroni, T. F. Stetina, M. Kieferova, C. O. Marrero, J. M. Arrazola, and N. Wiebe, arXiv [10.48550/arXiv.2210.05489](https://arxiv.org/abs/10.48550/arXiv.2210.05489) (2023).
- [24] A. Szabo and N. S. Ostlund, *Modern Quantum Chemistry: Introduction to Advanced Electronic Structure Theory* (Dover Publications, 1996).
- [25] R. J. Bartlett and M. Musiał, *Rev. Mod. Phys.* **79**, 291 (2007).
- [26] C. Møller and M. S. Plesset, *Phys. Rev.* **46**, 618 (1934).
- [27] W. Kohn, A. D. Becke, and R. G. Parr, *J. Phys. Chem.* **100**, 12974–12980 (1996).
- [28] B. L. Hammond, W. A. Lester, Jr., and P. J. Reynolds, *Monte Carlo Methods in Ab Initio Quantum Chemistry* (World Scientific, 1994).
- [29] S. R. White, *Phys. Rev. Lett.* **69**, 2863 (1992).
- [30] G. K.-L. Chan and S. Sharma, *Annu. Rev. Phys. Chem.* **62**, 465 (2011).
- [31] E. Farhi, J. Goldstone, S. Gutmann, and M. Sipser, arXiv [10.48550/arXiv.quant-ph/0001106](https://arxiv.org/abs/10.48550/arXiv.quant-ph/0001106) (2000).
- [32] S. McArdle, T. Jones, S. Endo, *et al.*, *npj Quantum Inf.* **5**, 75 (2019).
- [33] M. Motta, W. Kirby, I. Liepuoniute, K. J. Sung, J. Cohn, A. Mezzacapo, K. Klymko, N. Nguyen, N. Yoshioka, and J. E. Rice, arXiv [10.48550/arXiv.2312.00178](https://arxiv.org/abs/10.48550/arXiv.2312.00178) (2023).
- [34] W. Kirby, M. Motta, and A. Mezzacapo, *Quantum* **7**, 1018 (2023).
- [35] J. T. Seeley, M. J. Richard, and P. J. Love, *J. Chem. Phys.* **137**, 224109 (2012).
- [36] U. Azad, Pennylane quantum chemistry datasets, <https://pennylane.ai/datasets/collection/qchem> (2023).
- [37] V. Bergholm and et al., arXiv [10.48550/arXiv.1811.04968](https://arxiv.org/abs/10.48550/arXiv.1811.04968) (2022).
- [38] I. von Glehn, J. S. Spencer, and D. Pfau, in *The Eleventh International Conference on Learning Representations* (2023).
- [39] B. Recht, C. Re, S. Wright, and F. Niu, in *Advances in Neural Information Processing Systems*, Vol. 24 (Curran Associates, Inc., 2011).
- [40] K. Fujii, K. Mizuta, H. Ueda, K. Mitarai, W. Mizukami, and Y. O. Nakagawa, *PRX Quantum* **3**, 010346 (2022).
- [41] Q. H. Tran, S. Kikuchi, and H. Oshima, *Phys. Rev. Res.* **6**, 023181 (2024).
- [42] Q. H. Tran, Y. Endo, and H. Oshima, arXiv [10.48550/arXiv.2407.02419](https://arxiv.org/abs/10.48550/arXiv.2407.02419) (2024).
- [43] dvgodoy, dl-visuals, <https://github.com/dvgodoy/dl-visuals> (2020), gitHub repository, accessed February 10, 2025.